

PHOTODIODE-BASED X-RAY BEAM-POSITION MONITOR WITH HIGH SPATIAL-RESOLUTION FOR THE NSLS-II BEAMLINES*

P. S. Yoon[†], NSLS-II, Brookhaven National Laboratory, Upton, NY 11973 USA

D. P. Siddons, NSLS, Brookhaven National Laboratory, Upton, NY 11973 USA

Abstract

We developed a photodiode-based monochromatic X-ray beam-position monitor (X-BPM) with high spatial resolution for the project beamlines of the NSLS-II. A ring array of 32 *Si* PIN-junction photodiodes were designed for use as a position sensor, and a low-noise HERMES4 ASIC chip was integrated into the electronic readout system. A series of precision measurements to characterize electrically the *Si*-photodiode sensor and the ASIC chip demonstrated that the inherent noise is sufficiently below tolerance levels. Following up modeling of detector's performance, including geometrical optimization using a Gaussian beam, we fabricated and assembled a first prototype. In this paper, we describe the development of this new state-of-the-art X-ray BPM along the beamline, in particular, downstream from the monochromator.

MOTIVATION

The end stations for user's experiments at NSLS-II are located far from the X-ray sources. Hence, a small number of displacement- and angular-errors in a radiation source can degrade the end experiments. Accordingly, there is a pragmatic demand for a novel X-ray beam-position monitor (X-BPM) with high spatial resolution. A suite of six project beamlines under design are to be commissioned in the NSLS-II infrastructure[1]. A new X-BPM system developed specifically for these beamlines will serve as a diagnostic device for aligning beamline components and for real-time monitoring of a series of the beamline optics elements. The beam shape changes during its transportation through various optical elements. Therefore, it is anticipated that the performance of the new X-BPM will be less dependent upon the beam optics. Moreover, the mode of operation should affect the beam as little as possible to meet the stringent requirements for beam stability.

PHOTODIODE-SENSOR DESIGN

Figure 1 depicts the ring array of 32 photodiode pads that were designed and fabricated at in-house facilities¹. Boron ions are implanted on the front side of the wafer through 1

kA oxide, forming a *p-n* junction[2]. Phosphorous ions are implanted on the back side to make an ohmic contact with the front side. All 32 pads, configured as a polar array, are positioned between an inner ring radius of 5,050 μm and an outer ring radius of 6,763 μm . The active surface area of each pad is about 2.0 (mm^2), and each photodiode is 470- μm thick. In the photoconductive mode, the photodiodes are operated with reverse bias voltage of about 100. Upon impinging on a scatterer as a source of fluorescence radiation, the incident X-ray beam scatters and isotropically illuminates the backside of the ring photodiode. The photon sensor was devised for both back-side and front-side illumination. Our first prototype adopts a scheme of forward scattering using a silicon-nitride (Si_3N_4) substrate metalized with different species such as *Cr*, *Ni*, *Ti*, and *Au*. As Fig. 2 illustrates, the next version will utilize a backward-scattering scheme, employing *bi*-HERMES4 configuration that will be implemented later in the electronic readout.

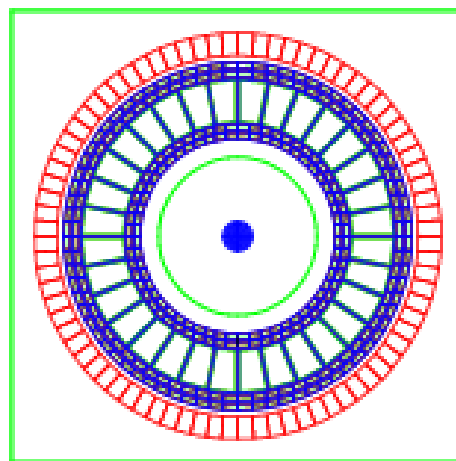


Figure 1: The ring array of segmented *Si* photodiodes. – drawing courtesy of the Instrumentation Division of BNL.

ELECTRICAL CHARACTERIZATION OF PHOTODIODE SENSOR

Achieving the desired level of detector performance requires a detailed electrical characterization of the optical sensor of the position-monitoring system. Hence, we undertook a comprehensive evaluation of each individual segment on the photodiode ring prior to completing the assem-

* This work was supported by the Department of Energy under contract number DE-AC02-98CH10886.

[†] yoon@bnl.gov

¹ There is a one-on-one correspondence between 32 pads and 32 ASIC channels.

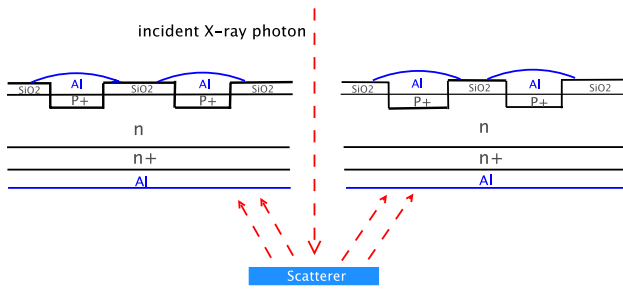


Figure 2: A schematic illustration of the backward-scattering scheme and the structure of the PIN-junction photodiode.

bly of our prototype detector. The inherent noise is reduced by reducing capacitance, followed by the segmentation of a photodiode array in parallel connections. I-V characteristics are acquired by sweeping the DC reverse-bias voltage, V_{rb} from 0 (V). One main design consideration for the ring-array *Si* photodiode is to ensure that most of an incident *X*-ray photon is absorbed within the depletion region of a reverse-biased junction. Because of the considerable width of depletion region (a few hundred μm), we selected the PIN junction. As shown in Fig. 3, leakage current measured from one pad is linear against the increasing reverse bias voltage on a log-log scale. Up to the operational bias voltage of 100 (V), the leakage current is held at the order of $n\text{A}$. As Fig. 4 shows, the depletion region is created at around 200 (V) from the *C-V* characteristic.

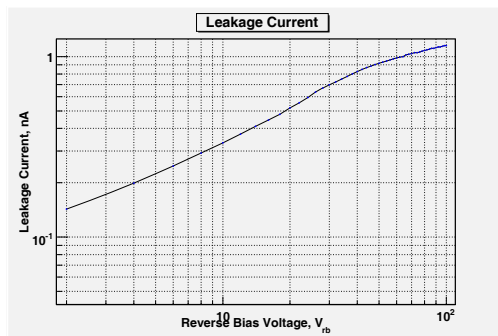


Figure 3: I-V characteristic curve.

GEOMETRICAL OPTIMIZATION

To maximize the detector's performance, an analytical model for optimizing its detector geometry was constructed. Because of the geometrical configuration of the ring-array photodiodes, the solid angle (Ω) [3, 4] of the photodiode sensor was calculated with parameterization as in Eqn. (1): In Fig. 5, the solid angle (Ω), which is an effective area seen by a beam, is plotted against the distance (Z^*) between the sensor and the fluorescence target. From our calculations, it was determined that an optimized working distance is 3.0 (mm) and the peak solid angle ($\hat{\Omega}$) is 0.76

02 BPMs and Beam Stability

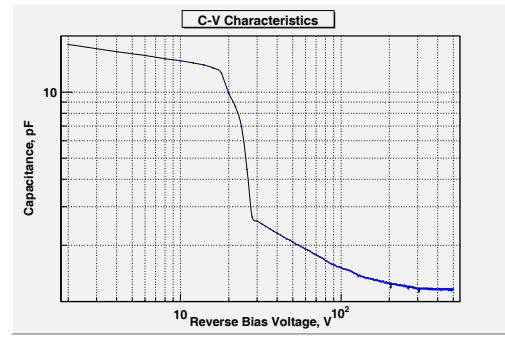


Figure 4: C-V characteristic curve.

(sr).

$$\begin{aligned}
 \Omega_{ring, \gamma} & \left(\underbrace{\rho^*, \theta^*, z^*}_{\text{beam parameters (3)}} ; \underbrace{\rho^+, \rho^-, \theta^+, \theta^-}_{\text{sensor parameters (4)}} \right) \\
 & = -\arctan \left[\frac{\Delta\theta^+ (\rho^{*2} - (\rho^* \rho^+) + z^{*2})}{z^* \sqrt{(\Delta\rho^+)^2 + (\rho^+ \Delta\theta^+)^2 + z^{*2}}} \right] \\
 & + \arctan \left[\frac{\Delta\theta^- (\rho^{*2} - (\rho^* \rho^+) + z^{*2})}{z^* \sqrt{(\Delta\rho^+)^2 + (\rho^+ \Delta\theta^-)^2 + z^{*2}}} \right] \\
 & + \arctan \left[\frac{\Delta\theta^+ (\rho^{*2} - (\rho^* \rho^-) + z^{*2})}{z^* \sqrt{(\Delta\rho^-)^2 + (\rho^- \Delta\theta^+)^2 + z^{*2}}} \right] \\
 & - \arctan \left[\frac{\Delta\theta^- (\rho^{*2} - (\rho^* \rho^-) + z^{*2})}{z^* \sqrt{(\Delta\rho^-)^2 + (\rho^- \Delta\theta^-)^2 + z^{*2}}} \right]
 \end{aligned} \quad (1)$$

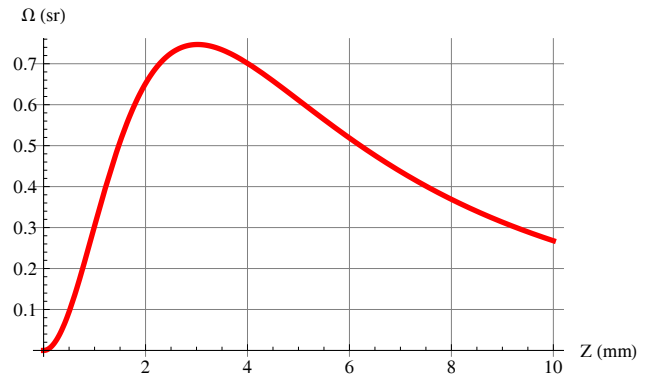


Figure 5: A plot of solid angle vs. working distance.

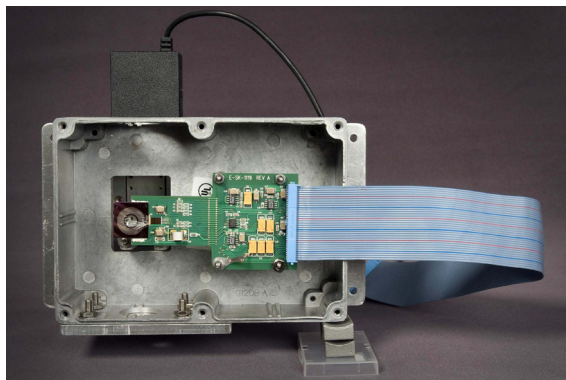
NEW ASIC DESIGN

We employed HERMES4, an application-specific integrated circuit (ASIC), which was redesigned at BNL for photon-counting application [5]. The new HERMES4 utilizing CMOS technology provides 32 channels, a charge pre-amplifier, a high-order charge shaper, a discriminators, an array of five 10-bit global DACs, and counters per channel. The HERMES4 was redesigned to read out input signals generated by the *Si*-photodiode sensor. The measured

electronic resolution is good, *viz.*, 15 rms e^- at a peaking time of 4 μsec . The gain settings available on HERMES4 are 750 mV/fC and 1,500 mV/fC . The settable peaking times are 0.5, 1, 2, and 4 μsec . Stray capacitance is reduced by direct *Al*-wire wedge-bonding between the 32 channels and sensor pads.

PROTOTYPE ASSEMBLY

As shown in Fig. 6, four linear stages are incorporated into the prototype detector. The two stages are for positioning the X-BPM in horizontal and vertical directions. The third one is for scanning a fluorescence source along the axial direction, and the last one is for setting a working distance between the photon sensor and the fluorescence target.



(a) an open enclosure.



(b) an assembled detector.

Figure 6: (a) An open enclosure of the new X-BPM. (b) a completely-assembled prototype detector.

BENCH-TOP MEASUREMENTS

Prior to beamline tests of the new X-BPM, we carried out bench-top measurements. After irradiation of the detector from a sealed radiation source of $Fe-55$, consistent signals were generated from each individual pad (Fig. 7), and registered with the ASIC chip.

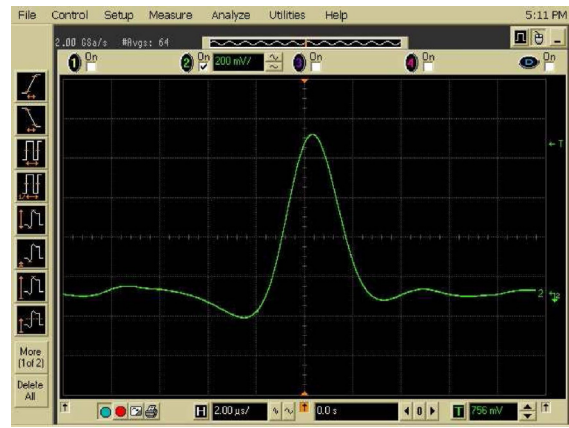


Figure 7: An example of a signal acquired after irradiation.

CLOSING REMARKS AND PLANS

Encouraged by the results from bench-top experiments and recent calibration runs on an existing beamline at NSLS, we are planning to undertake more detailed experiments to measure position sensitivity. Our analytical modeling enables us to predict the detector's performance in advance, and to develop enhanced photodiode sensors with larger solid angles. As a result, the new photodiode sensors will be used for the next version of prototypes.

ACKNOWLEDGMENTS

The authors gratefully acknowledge the support and provisions of the NSLS-II Experimental Facility Division, the NSLS Experimental Systems, and the Instrumentation Division of BNL.

REFERENCES

- [1] NSLS-II Conceptual Design Report, BNL-77977-2006-V1-V2, December 2006
- [2] Z. Li, and W. Chen *priv. comm.*, Brookhaven National Laboratory, 2009
- [3] R. Alkire, "Design of Vacuum-Compatible High-Precision Monochromatic Beam-Position Monitor for Use with Synchrotron Radiation from 5 to 25 keV ", *J. of Synchrotron Rad.*, 2001, **7**
- [4] C. DeCusatis, "Handbook of Applied Photometry", AIP Press, New York, 1997
- [5] G. De Geronimo et al., "Readout ASIC for 3D Position-Sensitive Detectors", 2007 IEEE Nuclear Science Symposium Conference Record, Brookhaven National Laboratory